



OPEN

CONFERENCE
PROCEEDINGSACSMS2014
.....

SUBJECT AREAS:

OPTICS AND PHOTONICS

ORGANIC LEDs

Received

1 September 2014

Accepted

29 October 2014

Published

19 November 2014

Correspondence and requests for materials should be addressed to J.F. (jifeng@jlu.edu.cn) or H.-B.S. (hbsun@jlu.edu.cn)

Surface Plasmon-Polariton Mediated Red Emission from Organic Light-Emitting Devices Based on Metallic Electrodes Integrated with Dual-Periodic Corrugation

Yan-Gang Bi¹, Jing Feng¹, Yu-Shan Liu¹, Yun-Fei Li¹, Yang Chen¹, Xu-Lin Zhang¹, Xiao-Chi Han¹ & Hong-Bo Sun^{1,2}

¹State Key Laboratory on Integrated Optoelectronics, College of Electronic Science and Engineering, Jilin University, 2699 Qianjin Street, Changchun, 130012, People's Republic of China, ²College of Physics, Jilin University, 119 Jiefang Road, Changchun, 130023, People's Republic of China.

We demonstrate an effective approach to realize excitation and outcoupling of the SPP modes associated with both cathode/organic and anode/organic interfaces in OLEDs by integrating dual-periodic corrugation. The dual-periodic corrugation consists of two set gratings with different periods. The light trapped in the SPP modes associated with both top and bottom electrode/organic interfaces are efficiently extracted from the OLEDs by adjusting appropriate periods of two set corrugations, and a 29% enhancement in the current efficiency has been obtained.

Due to the promising applications in full-color flat-panel displays and solid-state lighting sources, organic light-emitting devices (OLEDs) have attracted considerable interests since their discoveries¹⁻⁶. Light extraction in OLEDs has been an active area of research because of significant power loss arising from substrate modes from the total internal reflection at the glass substrate/air interface, waveguide (WG) modes in organic/indium-tin-oxide (ITO) anode layers, and surface plasmon-polariton (SPP) modes associated with the metallic electrode/organic interface⁷⁻⁹. The low light outcoupling (less than 20%) has become one of the main limitations to high efficiency of the OLEDs for commercial applications¹⁰⁻¹². There is still the greatest scope for significant improvements in efficiency through an efficient recover of the lost power. It can be easily realized for Light extraction of the substrate modes by attaching a microlens array on the outside of the substrate^{13,14}. Using metallic anode, for example, thin metal film, metal grid or metal nanowires with high optical transmission and electrical conductivity as a direct replacement for ITO has a potential to recover the power loss to the WG modes in ITO¹⁵⁻¹⁹. OLEDs with metallic films as both top cathode and bottom anode by employing semitransparent Au thin films as anode have shown superior device performance^{8,20}. In this case, light trapped in the SPP modes existed at cathode/organic interface and anode/organic interface become the main power loss, and therefore, highly efficient light extraction could be expected by excitation and outcoupling of the SPP modes associated with both top and bottom electrode/organic interfaces in the OLEDs.

Introducing a wavelength-scale nanostructure onto the metallic electrode surface has exhibited its remarkable effect for excitation and outcoupling of the SPP modes by providing an additional momentum to couple the SPP modes into light²¹⁻²³. A periodic nanostructure is suitable for specific narrow range of wavelength by satisfying the Bragg scattering condition²⁰. While, the SPP resonant wavelength would be different for the cathode and anode interfaces due to the different metal materials are used, so that the excitation and outcoupling of the SPP modes can be realized only at one of the electrode interfaces^{23,24}. Therefore, recovering the power loss to SPPs at both cathode and anode interfaces simultaneously is an important issue to further improve the efficiency of the OLEDs. In this communication, efficient excitation and outcoupling of the SPP modes associated with both top and bottom electrode/organic interfaces has been realized by introducing a two-dimensional (2D) grating with dual-periodic corrugation into the OLEDs. The 2D grating consists of two set corrugations with different periods. The



SPP resonance at the cathode/organic and anode/organic interfaces can be tuned to the same wavelength to coincide with the electroluminescent (EL) peak of the OLEDs by adjusting appropriate periods of the two set corrugations. As a result, the light trapped in the SPP modes associated with the two electrode/organic interfaces are both efficiently extracted from the OLEDs respectively. A 29% enhancement in the current efficiency compared to those of the conventional planar devices has been obtained.

Results and Discussion

The schematic experimental realization of the dual-periodic corrugated OLEDs with efficient excitation and outcoupling of the SPP modes associated with both top and bottom electrode/organic interfaces has been shown in Figure 1. The periodic corrugations were fabricated on a photoresist layer spin-coated on the pre-cleaned glass substrates by a laser interference lithography (LIL) technique²⁵. The dual-periodic corrugation has two set gratings with different periods and rotated 90° with respect to each other. 1D and 2D mono-periodic corrugations were also prepared by the same technology for comparison. Their morphologies on the photoresist surface were investigated by atomic force microscopy (AFM), and shown in Figure 1 and Figure S1 in supporting information. The groove depth was about 60 nm for the periodic corrugation by tuning the laser fluence²⁶. A red OLED was fabricated on the corrugated substrate based on a red-emitting phosphorescent material Bis(2-methyl-dibenzo[*f,h*]quinoxaline) (acetylacetonate) iridium (III) [(MDQ)₂Ir(acac)] as described in methods section²⁷.

SPPs are electromagnetic excitations propagating at the interface between a dielectric and a conductor, evanescently confined in the perpendicular direction²⁸. It is well known that SPPs can be optically excited by incident radiation if the metal surface in which the SPPs reside shows a periodic corrugation to satisfy conversion of energy and momentum^{28–30}. SPP resonance at the corrugated metal surface can be tuned by adjusting the grating periods^{23,24}. Its consistency with the emitting wavelength of the OLEDs is crucial for the efficient outcoupling of the SPP modes. Au and Ag are chosen as top cathode and bottom anode, respectively. The structure of the corrugated OLEDs is Au (15 nm)/MoO₃ (5 nm)/CBP (60 nm)/CBP:(MQD)₂Ir(acac) (20 nm, 8% wt)/Bphen (10 nm)/Alq₃ (20 nm)/Ca (2 nm)/Ag (80 nm), and the emission wavelength for the OLEDs is located at around 605 nm (Figure S2, supporting information), which are from the emission of the red emitter (MQD)₂Ir(acac). Absorption spectra associated with cathode/organic and anode/organic interfaces with various corrugation periods were measured to determine the optimized periods as shown in Figure 2. A number

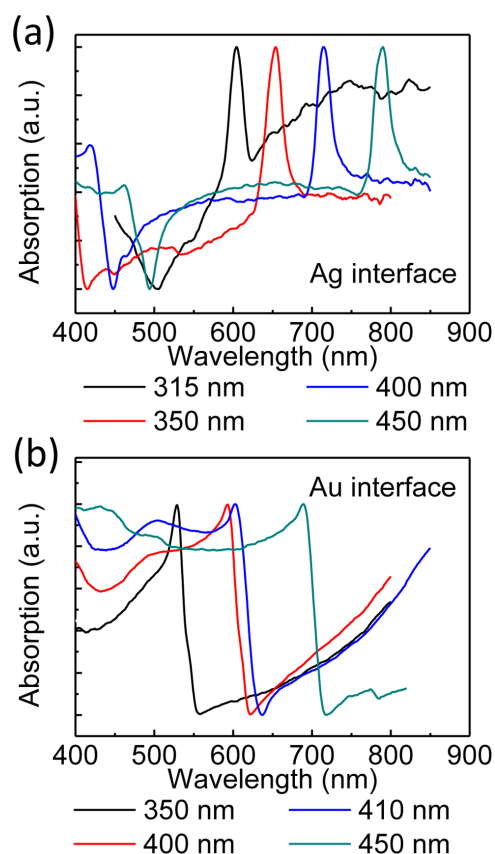


Figure 2 | Absorption spectra of the OLED structures with various periods of 1D corrugation.

of absorption maxima could be seen, if the incident light is coupled into the SPPs supported by the structure. In order to investigate the two electrode/organic interfaces individually, the structure of the device engaged for the absorption spectra measurement associated with Ag cathode/organic interface was CBP/CBP:(MQD)₂Ir(acac)/Bphen/Alq₃/Ca/Ag, while the structure for the measurement of the Au anode/organic interface was engaged to be Au/MoO₃/CBP/CBP:(MQD)₂Ir(acac)/Bphen/Alq₃. More specifically, planar devices with the same structures were used as the reference samples for the absorption measurement to exclude the absorption by the planar metal and organic films at the observed wavelength region, so that

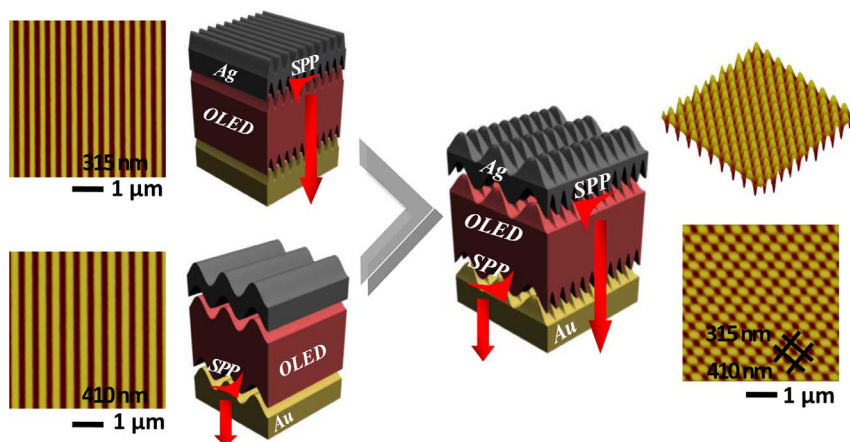


Figure 1 | Schematic of excitation and outcoupling of the SPP modes associated with both cathode/organic and anode/organic interfaces in OLEDs by engaging dual-periodic corrugation, and AFM images of surface morphologies of photoresist with 1D period of 315 nm (top left) and 325 nm (lower left), and 2D dual-periodic corrugation (right-hand side), respectively.



the peaks originated from the SPP resonance supported by the periodic corrugation could be distinguished clearly. The thickness of the Ag cathode is decreased from 80 to 50 nm for the absorption measurement, and Au anode keeps at 15 nm. The SPP resonance of around 605 nm is desired for both top and bottom electrode interfaces according to the emission wavelength of the OLED. The wavelength of the absorption peak at normal direction increases with the corrugation period for both Ag and Au interfaces. Therefore, the favorable periods of the corrugations were determined to be 315 nm for the Ag/organic interface and 410 nm for the Au/organic interface, respectively, since they both correspond to a SPP resonance of 605 nm. The angular-dependent absorption spectra as the function of the observation angle for the 1D 315 nm corrugated and 1D 410 nm corrugated devices were also measured and shown in Figure S3 in supporting information, in which the absorption peak splits into two peaks, which move to lower and higher wavelengths, respectively, with the increased observation angle. The peak splitting behavior is typical of Bragg diffraction of surface waves or guided modes.

After determined the periods of the corrugations, the two periods of 315 and 410 nm are combined to form the dual-periodic corrugation. The absorption spectra of the dual-periodic corrugated devices associated with the Ag/organic interface and Au/organic interface have been measured as shown in Figures 3a and b. Two absorption maxima can be observed in each spectrum, which is arising from the two different periods of the dual-periodic corrugations. A peak at around 605 nm can be observed in both cases. Figures 3c and d show the angular-dependent absorption spectra of the dual-periodic corrugated devices under a transverse-magnetic (TM) and transverse-electric (TE) polarized light source. We should note that the incidence with the electric and magnetic component vertical to the xz plane can be called as TE and TM polarized incidence, respectively. Different from the spectra under nonpolarized incident light, only one absorption peak around 605 nm can be observed at normal direction under the polarized incident light. The spectra for the TM polarized absorption coincides with that of the 1D corrugated devices with 315 nm period (Figure S3a), which demonstrates that it is originated from the SPP modes associated with the Ag cathode/

organic interface supported by the 315 nm period of corrugation. While the TE polarized absorption coincides with the 1D corrugated OLEDs with 410 nm period (Figure S3b), and therefore, is arising from the SPP modes associated with the Au anode/organic interface supported by the 410 nm period of corrugation. In case of the Ag/organic interface, an additional peak at around 750 nm can be observed in the nonpolarized absorption spectrum, which is from the SPP resonance corresponding to the corrugation period of 410 nm, and is far from the desired wavelength of the red emission. The additional peak appears at around 500 nm in case of the Au/organic interface, which is from the SPP resonance corresponding to the corrugation period of 315 nm, and is also far from the desired wavelength of the red emission. These data demonstrates clearly that dual-periodic corrugation is necessary to tune the SPP resonance of the Ag/organic and Au/organic interfaces to the same wavelength. The above results indicate that the dual-periodic corrugation with periods of 315 nm and 410 nm is favorable for efficient light extraction from the red-emitting OLEDs.

In-house generated finite-difference time-domain (FDTD) code is applied to simulate the absorption spectra to confirm the excitation and outcoupling of the SPPs^{20,29}. The theoretically calculated absorption spectra of the OLEDs integrated with 1D mono-periodic corrugation with various grating periods are shown in Figure S5 in supporting information, in which the peak positions are identical with the measured spectra (Figure 2). The simulated dispersion maps with TM and TE polarized incident light associated with two different metal/organic interfaces are shown in Figures 4a and b, in which the absorption intensity is as a function of both incident angle and absorption wavelength. Dispersion relations constructed from the measured absorption spectra with TM and TE polarization (Figures 3c and d) are also plotted in Figures 4a and b. It can be seen that there is an excellent agreement between the numerically calculated and experimentally measured dispersion relations. The spatial steady-state H_z field intensity distributions across the device structure as a function of position with the normal incident light are calculated for the device with the dual-periodic corrugation in order to identify the optical modes supported by the corrugated OLEDs. Figure 4c shows the field intensity distributions associated with Ag/organic interface for the TM-polarized incidence with a wavelength of 605 nm. The field intensity exhibits its maxima at the Ag/organic interface and decays along the direction perpendicular to it, which demonstrates that the absorption peak at 605 nm originates from SPP modes, since SPPs are surface wave and propagating along the interface between a metal and a dielectric^{24,30}. In case of the TE polarized incidence with a wavelength of 605 nm, the field intensity exhibits its maxima at the Au/organic interface as shown in Figure 4d, which demonstrates the excitation of the SPP modes associated with the Au/organic interface. The above numerical simulations confirm the excitation and outcoupling of the SPP modes from both top and bottom metal/organic interfaces in the dual-periodic corrugated devices.

To investigate the effect of the dual periodic corrugation on the light extraction from the OLEDs, the EL performances of the 1D or 2D mono-periodically corrugated, dual-periodically corrugated and planar OLEDs have been compared and summarized in Figure 5 and Table S1 in supporting information, respectively. The dual-periodically corrugated OLEDs show obvious enhancement in both luminance and efficiency as expected. The maximum luminance increases from 12470 cd/m² for the planar device to 20470 cd/m² for the 1D 315 nm periodic device, 24130 cd/m² for the 1D 410 nm periodic device, 31650 cd/m² for the 2D 315 nm mono-periodic device, 35560 cd/m² for the 2D 410 nm mono-periodic device, and 47950 cd/m² for the dual-periodic device, respectively. The maximum current efficiency is improved from 17.98 cd/A for the planar device to 19.38 cd/A for the 1D 315 nm periodic device, 20.46 cd/A for the 1D 410 nm periodic device, 20.27 cd/A for the 2D 315 nm

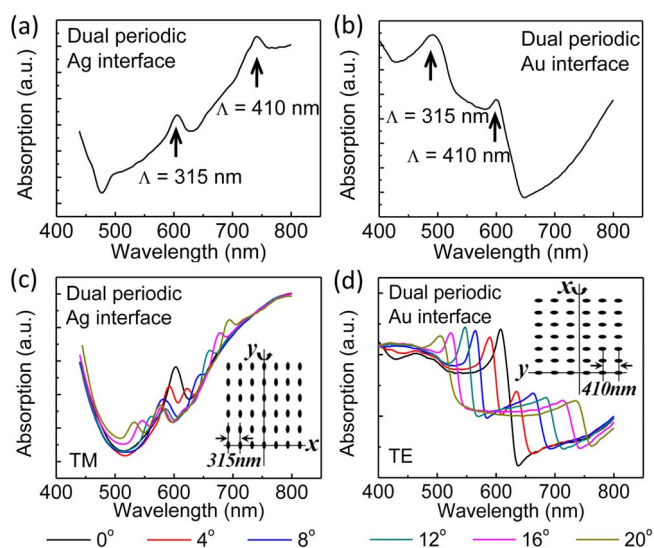


Figure 3 | (a) – (b) Absorption spectra of the OLED structures with 2D dual-periodic corrugated Ag/organic and Au/organic interfaces, respectively. (c) – (d) Angular dependent absorption spectra of the dual-periodic corrugated OLEDs from 0° to 20° under TM and TE polarized incident light source at different rotation axes, respectively. The insets in (c) and (d) show the orientation of rotation axis. The rotation axis is parallel to one of the grooves for the 2D corrugation of the nanostructure, respectively.

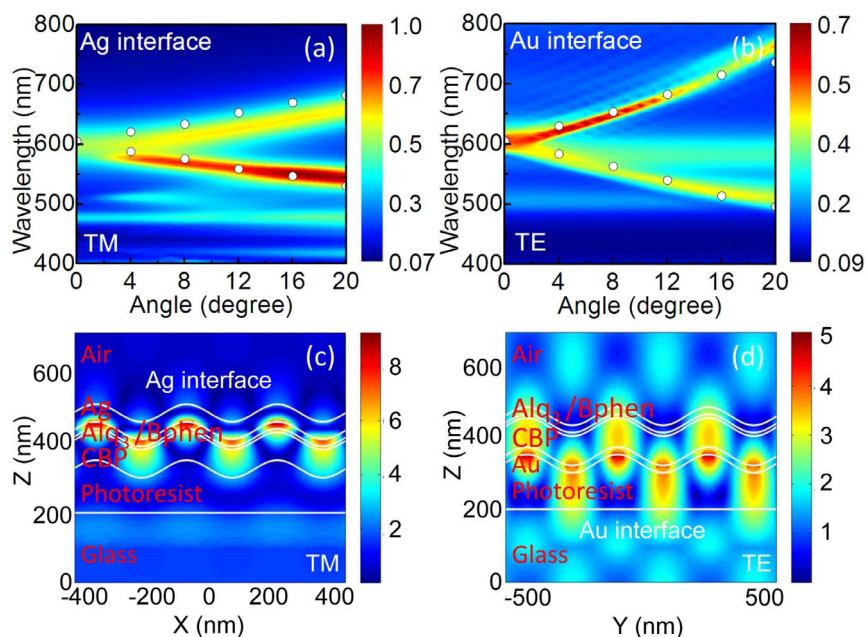


Figure 4 | Calculated dispersion relations for the wavelength versus incident angle of the dual-periodic sample under TM polarization associated with Ag/organic interface (a) and TE polarization associated with Au/organic interface (b), and distributions of the magnetic field intensity across the dual-periodic sample with the normal incident light at the wavelength of 605 nm with TM polarization associated with Ag/organic interface (c) and TE polarization associated with Au/organic interface (d). The measured dispersion relations extracted from the absorption spectra (circles) are also shown in (a) and (b).

periodic device, 21.09 cd/A for the 2D 410 nm periodic device, and 23.22 cd/A for the dual-periodic corrugated device, respectively. The 1D mono-periodic corrugated devices reveal 7.79% (315 nm period) and 13.79% (410 nm period) enhancement in the current efficiency, and the 2D mono-periodic corrugated devices reveal 12.74% (315 nm period) and 17.30% (410 nm period) enhancement compared to those of the conventional planar device, while it reveals a 29.14% enhancement in the current efficiency by integrating the dual-periodic corrugations.

Understanding the enhancement mechanism can be obtained by analyzing the optical modes within the dual-periodic corrugated OLEDs by measuring its emission spectra as a function of observation angle. Figure 6 shows the EL spectra measured from the dual-periodically corrugated OLEDs at several observation angles to the surface. The additional peaks in the TM and TE polarized EL spectra and their shifts in wavelength as the angle varies can be clearly observed in Figures 6a and b. Compared with the polarized absorption spectra (Figures 3a and b), their peak wavelengths are almost coincident, which demonstrates an efficient outcoupling of the photons from the trapped SPP modes associated with both the cathode/organic and anode/organic interfaces. However, the bandwidth of the EL spectra is different from the absorption spectra on the account of that the fluorescence of $(\text{MDQ})_2\text{Ir}(\text{acac})$ may decide the bandwidth of the EL emission. Angular dependent EL spectra with TM and TE polarization of 1D mono-periodically corrugated OLED are also measured and compared with the measured absorption spectra to verify the outcoupling of the SPP modes, as shown in Figure S6 in supporting information. Combining with the above experimental and numerical results, the EL enhancement could be attributed to the light extraction by the excitation and radiation of the SPP modes at both of the cathode/organic and anode/organic interfaces by integrating the dual-periodic corrugation.

Conclusions

In summary, we demonstrate an effective approach to realize a light extraction enhancement in OLEDs by introducing dual-periodic

corrugation into metallic electrodes. The dual-periodic corrugation has the effect to outcouple the power lost to the SPP modes associated with both cathode/organic and anode/organic interfaces in the re-emitting OLEDs. A significantly enhanced EL efficiency from the dual-periodic corrugated OLEDs has been observed, and a 29% enhancement in current efficiency compared to those of the conventional planar devices has been obtained. The employing of the dual-periodic corrugation in the OLEDs has opened an avenue to enhance the efficiency, which has the potential in the commercial applications of the OLEDs.

Methods

Fabrication of the Dual Periodic Corrugation: The laser interference lithography technique was employed to fabricate the periodic corrugations. By adjusting the angle of the two laser beams, the nanostructures with various periods can be obtained. The photoresist (NOA63, Norland Products, Inc.) diluted in acetone at a concentration of 25 mg/ml was spin coated on the pre-cleaned glass substrate at a concentration of 25 mg/ml was spin coated on the pre-cleaned glass substrate at 6000 rpm speed for 20 s. The thickness of photoresist film was 100 nm. A continuous laser with 266 nm wavelength (Coherent Inc.) was used as irradiance light source for the lithography. The sample was exposed by two laser beams which were split from the UV laser with a beam size of ~ 6 mm in diameter. 1D mono-periodic grating was obtained by exposing the photoresist to the interference fringes. For the fabrication of the dual-periodic corrugation, the sample was exposed for the second time after rotation of 90° with a different writing angle. The nanostructure with different periods and depths can be obtained by adjusting the writing angle and the exposure time. The morphologies of the nanostructure were characterized by an atomic force microscopy (AFM, Dimension Icon, Bruker Corporation) in the tapping mode.

OLEDs Fabrication and Evaluation: Glass substrates coated with corrugated photoresist film were immediately loaded into a thermal evaporation chamber. A 15 nm semitransparent Au anode was deposited on the prepared substrates. A 5 nm MoO_3 anodic modification layer, 60 nm thick hole-transporting layer of 4,40-bis(-carbazol-9-yl)biphenyl (CBP), 20 nm thick emitting layer of 8% wt Bis(2-methyl-dibenzo[*f,h*]quinoxaline) (acetylacetonate) iridium (III) [$(\text{MDQ})_2\text{Ir}(\text{acac})$] doped into CBP, 10 nm hole-blocking layer of 4,7-diphenyl-1,10-phenanthroline (Bphen), 20 nm electron-transporting layer of tris-(8-hydroxyquinoline) aluminum (Alq_3), and cathode of Ca (2 nm)/Ag (80 nm) were evaporated sequentially at a base pressure of 5×10^{-4} Pa. The absorption spectra were measured by UV-Vis spectrophotometer (UV-2550, SHIMADZU). The angular dependent electroluminescent spectra were measured by a fiber optic spectrometer. A slit was used to limit the angular acceptance to $\sim 1^\circ$, and the OLEDs were placed on a rotation stage with grooves (one of the grooves for the 2D corrugation) parallel to the rotation axis. The voltage-current density and current density-luminance characteristics of the devices were measured

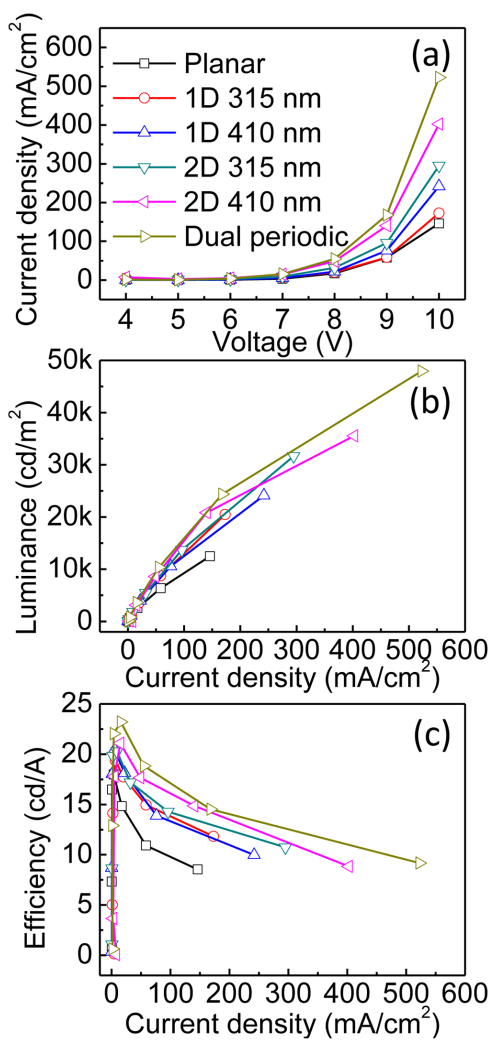


Figure 5 | EL performance of the corrugated and planar OLEDs. Voltage-current density (a), current density-luminance (b) and current density-efficiency (c) characteristic curves of the corrugated and planar OLEDs.

by Keithley 2400 programmable voltage-current source and Photo Research PR-655 spectrophotometer. The active area of the device is 2×2 mm². All of the measurements were conducted in air at room temperature.

- Reineke, S. *et al.* White organic light-emitting diodes with fluorescent tube efficiency. *Nature* **459**, 234–238 (2009).
- Liu, Y. P. *et al.* “Quasi-freestanding” graphene-on-single-walled carbon nanotube electrode for applications in organic light-emitting diode. *Small* **10**, 944–949 (2014).
- Zhang, S., Turnbull, G. A. & Samuel, I. D. W. Highly directional emission and beam steering from organic light-emitting diodes with a substrate diffractive optical element. *Adv. Opt. Mat.* **2**, 343–347 (2014).
- Gross, M. *et al.* Improving the performance of doped pi-conjugated polymers for use in organic light-emitting diodes. *Nature* **405**, 661–665 (2000).
- Mastroradi, M. L. *et al.* Silicon nanocrystal LEDs: Effect of organic capping group on performance. *Small* **8**, 3647–3654 (2012).
- Sun, Y. R. *et al.* Management of singlet and triplet excitons for efficient white organic light-emitting devices. *Nature* **440**, 908–912 (2006).
- Kim, J. B., Lee, J. H., Moon, C. K., Kim, S. Y. & Kim, J. J. Highly enhanced light extraction from surface plasmon loss minimized organic light-emitting diodes. *Adv. Mater.* **25**, 3571–3577 (2013).
- Bi, Y. G. *et al.* Enhanced efficiency of organic light-emitting devices with metallic electrodes by integrating periodically corrugated structure. *Appl. Phys. Lett.* **100** (2012).
- Choi, C. S. *et al.* Blur-free outcoupling enhancement in transparent organic light-emitting diodes: A nanostructure extracting surface plasmon modes. *Adv. Opt. Mat.* **1**, 687–691 (2013).

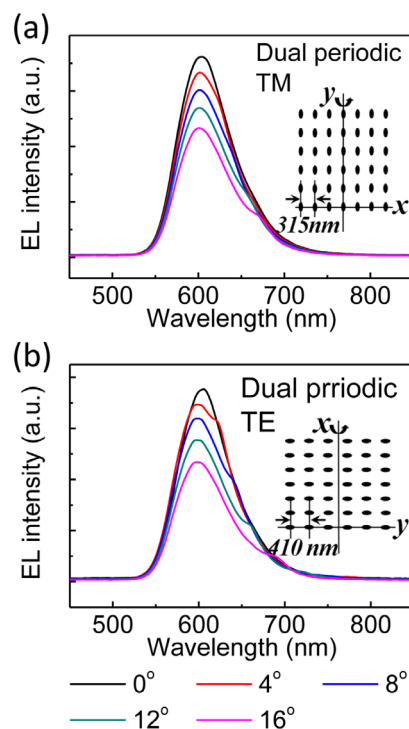


Figure 6 | EL spectra at different observation angles of the dual-periodic-corrugated OLED with different orientations of the rotation axis under TM polarization (a) and TE polarization (b). The insets show the orientation of the rotation axis.

- Koo, W. H. *et al.* Light extraction from organic light-emitting diodes enhanced by spontaneously formed buckles. *Nat. Photonics* **4**, 222–226 (2010).
- Jiang, Y., Chen, S., Li, G., Li, H. & Kwok, H.-S. A low-cost nano-modified substrate integrating both internal and external light extractors for enhancing light out-coupling in organic light-emitting diodes. *Adv. Opt. Mat.* **2**, 418–422 (2014).
- Forrest, S. R. The road to high efficiency organic light emitting devices. *Org. Electron.* **4**, 45–48 (2003).
- Eom, S.-H., Wrzesniewski, E. & Xue, J. Close-packed hemispherical microlens arrays for light extraction enhancement in organic light-emitting devices. *Org. Electron.* **12**, 472–476 (2011).
- Möller, S. & Forrest, S. R. Improved light out-coupling in organic light emitting diodes employing ordered microlens arrays. *J. Appl. Phys.* **91**, 3324–3327 (2002).
- De, S. *et al.* Silver nanowire networks as flexible, transparent, conducting films: Extremely high dc to optical conductivity ratios. *ACS Nano* **3**, 1767–1774 (2009).
- Helander, M. G. *et al.* Oxidized gold thin films: An effective material for high-performance flexible organic optoelectronics. *Adv. Mater.* **22**, 2037–2040 (2010).
- Kuang, P. *et al.* A new architecture for transparent electrodes: Relieving the trade-off between electrical conductivity and optical transmittance. *Adv. Mater.* **23**, 2469–2473 (2011).
- Wu, H. *et al.* Electrospun metal nanofiber webs as high-performance transparent electrode. *Nano Lett.* **10**, 4242–4248 (2010).
- Chiappe, D., Toma, A. & de Mongeot, F. B. Transparent plasmonic nanowire electrodes via self-organized ion beam nanopatterning. *Small* **9**, 913–919 (2013).
- Bi, Y. G. *et al.* Broadband light extraction from white organic light-emitting devices by employing corrugated metallic electrodes with dual periodicity. *Adv. Mater.* **25**, 6969–6974 (2013).
- Ozbay, E. Plasmonics: Merging photonics and electronics at nanoscale dimensions. *Science* **311**, 189–193 (2006).
- Jin, Y. *et al.* Solving efficiency-stability tradeoff in top-emitting organic light-emitting devices by employing periodically corrugated metallic cathode. *Adv. Mater.* **24**, 1187–1191 (2012).
- Yates, C. J., Samuel, I. D. W., Burn, P. L., Wedge, S. & Barnes, W. L. Surface plasmon-polariton mediated emission from phosphorescent dendrimer light-emitting diodes. *Appl. Phys. Lett.* **88** (2006).
- Andrew, P. & Barnes, W. L. Energy transfer across a metal film mediated by surface plasmon polaritons. *Science* **306**, 1002–1005 (2004).
- Yang, J. *et al.* Design and fabrication of broadband ultralow reflectivity black Si surface by laser micro/nanoprocessing. *Light: Sci. Appl.* **3**, e185 (2014).
- Zhang, X. L., Feng, J., Song, J. F., Li, X. B. & Sun, H. B. Grating amplitude effect on electroluminescence enhancement of corrugated organic light-emitting devices. *Opt. Lett.* **36**, 3915–3917 (2011).



27. Chang, Y. L. *et al.* Enhancing the efficiency of simplified red phosphorescent organic light emitting diodes by exciton harvesting. *Org. Electron.* **13**, 925–931 (2012).
28. Maier, S. A. *Plamonics: Fundamentals and Applications*. (Springer, New York, 2007).
29. Bai, Y. *et al.* Outcoupling of trapped optical modes in organic light-emitting devices with one-step fabricated periodic corrugation by laser ablation. *Org. Electron.* **12**, 1927–1935 (2011).
30. Barnes, W. L., Dereux, A. & Ebbesen, T. W. Surface plasmon subwavelength optics. *Nature* **424**, 824–830 (2003).

Acknowledgments

The authors gratefully acknowledge support from the 973 Project (2013CBA01700), NSFC (Grant Nos. 61322402, 91233123 and 61177024), and Graduate Innovation Fund of Jilin University (2014022).

Author contributions

Y.G.B., J.F. and H.B.S. conceived the study; X.L.Z. and X.C.H. helped with the theoretical

analysis; Y.G.B., Y.S.L., Y.F.L. and Y.C. did most of the experiments; Y.G.B., J.F. and H.B.S. analyzed the data and wrote the manuscript.

Additional information

Supplementary information accompanies this paper at <http://www.nature.com/scientificreports>

Competing financial interests: The authors declare no competing financial interests.

How to cite this article: Bi, Y.-G. *et al.* Surface Plasmon-Polariton Mediated Red Emission from Organic Light-Emitting Devices Based on Metallic Electrodes Integrated with Dual-Periodic Corrugation. *Sci. Rep.* **4**, 7108; DOI:10.1038/srep07108 (2014).



This work is licensed under a Creative Commons Attribution-NonCommercial-NoDerivs 4.0 International License. The images or other third party material in this article are included in the article's Creative Commons license, unless indicated otherwise in the credit line; if the material is not included under the Creative Commons license, users will need to obtain permission from the license holder in order to reproduce the material. To view a copy of this license, visit <http://creativecommons.org/licenses/by-nc-nd/4.0/>